Journal of Power Sources 195 (2010) 3858–3869

Contents lists available at ScienceDirect

Journal of Power Sources

journal homepage: www.elsevier.com/locate/jpowsour

Fundamental characterization of evaporative water removal from fuel cell diffusion media

Kyu Taek Cho, Matthew M. Mench*

Fuel Cell Dynamics and Diagnostics Laboratory, Department of Mechanical and Nuclear Engineering, The Pennsylvania State University, University Park, PA 16802, United States

ARTICLE INFO

Article history:
Received 4 November 2009
Received in revised form
17 December 2009
Accepted 17 December 2009
Available online 28 December 2009

Keywords:
Polymer electrolyte fuel cell
Diffusion media
Purge
Evaporation
Funicular regime
Pendular regime

ABSTRACT

In polymer electrolyte fuel cell systems, a gas purge commonly is applied to remove excess water and achieve high performance and durability. The porous diffusion media (DM) typically store a significant fraction of the total liquid water during operation, but quantitative fundamental research examining water removal behavior from DM is not yet available in literature. The objective of this study is to investigate the fundamental behavior of evaporative water removal from fuel cell diffusion media with a special test rig developed to minimize in-plane gradients so that through-plane evaporative behavior can be analyzed. Evaporative water removal was characterized by a surface evaporation region, a constant evaporation rate region characterized by capillary flow to the evaporation front, and a falling rate region characterized by separated evaporating droplets. A semi-empirical correlation for the characteristic water removal, a generic plot of purge efficiency which describes the effectiveness of purge parameters, and a potential scheme for a more durable and less parasitic purge which describes characteristic water removal of each fuel cell component were developed. The results of this study can be used to predict and understand water removal from diffusion media and help develop a less parasitic purge protocol than presently utilized.

1. Introduction

Cold start performance and durability of polymer electrolyte fuel cells (PEFC) can be compromised if residual liquid water is not removed from the fuel cell after shutdown [1]. Extensive research has been conducted to minimize the residual water by methods including gas purge [2–4], vacuum evaporation [5], and temperature-driven water drainage [6,7]. A direct and parasitic gas purge is generally utilized in most practical applications, however it is highly parasitic, and reduces the overall system efficiency, especially considering a typical drive cycle with many short trips. It is therefore desired to understand evaporative behavior in the channel and porous media, so that protocol, materials, and design can be optimized to reduce this parasitic loss. High frequency resistance (HFR) has been used to monitor the status of water content during gas purge under the assumption of sequential drying in components, starting from flow field plate, diffusion media (DM), and finally to membrane electrolyte assembly (MEA) [2–4]. However, Cho et al. determined from experiment using HFR combined with neutron radiography (NR) that in most cases, sequential drying is not a proper assumption [8]. HFR indicates the overall dryness of membrane, and NR accurately quantifies the total liquid water amount in all the components in the cell including flow field plate, DM and MEA. Membrane water content was found to vary somewhat independently of the total water amount in the cell, rather than sequentially, as purge progressed. However, it is not possible to only remove water from the catalyst layer or membrane without first removing some water from the diffusion media. Therefore, the water removal behavior of each component during purge must be more fundamentally understood to enable a thorough purge of flow field plate and DM without excessive drying of the membrane, which has been shown to result in accelerated degradation [2]. It is also desired to perform such a study *ex situ*, with minimal in-plane gradients in temperature, relative flow humidity above the sample, and saturation, so that the intrinsic evaporative processes can be better understood and not confounded with a particular cell design.

Extensive work has been conducted to understand water removal behavior from the flow field plate, DM, and MEA [4,9–12]. However, fundamental understanding of water evaporation from the DM is still unavailable in the literature, even though DM typically stores a significant fraction of the total liquid water in the operating fuel cell [11], and removal of some of this is necessary to dry the CL and CL|MPL interface to acceptable levels. By understanding the characteristic water removal of DM during gas purge, an optimized purge protocol can be developed with minimal parasitic energy requirement and no degradation of components.

* Corresponding author. Tel.: +1 814 865 0060; fax: +1 814 863 4848.
E-mail address: mmm124@psu.edu (M.M. Mench).

0378-7753/$ – see front matter © 2009 Elsevier B.V. All rights reserved.
doi:10.1016/j.jpowsour.2009.12.084

Nomenclature

A	area (m^2)
c_p	heat capacity ($kJ\,kg^{-1}\,K^{-1}$)
D	binary diffusion coefficient ($m^2\,s^{-1}$)
D_h	hydraulic diameter (m)
d	pore diameter (m)
f	friction factor
h	enthalpy ($kJ\,kg^{-1}$)
$\underline{h_{conv}}$	heat transfer coefficient ($W\,m^{-2}\,K^{-1}$)
$\overline{h_{conv}}$	average heat transfer coefficient ($W\,m^{-2}\,K^{-1}$)
h_{lg}	latent heat of vaporization ($kJ\,kg^{-1}$)
$\underline{h_m}$	mass transfer coefficient ($m\,s^{-1}$)
$\overline{h_m}$	average mass transfer coefficient ($m\,s^{-1}$)
K	absolute permeability (m^2)
k_r	relative permeability
k_t	thermal conductivity ($W\,m^{-1}\,K^{-1}$)
L	length (m)
Le	Lewis number
m	mass (kg)
$\dot{m}$	mass flow rate ($kg\,s^{-1}$)
$\bar{\dot{m}}$	average mass flow rate ($kg\,m^{-1}\,s^{-1}$)
P	pressure (Pa)
$\dot{q}$	heat transfer rate (W)
q''	heat flux ($W\,m^{-2}$)
Re	Reynolds number
s	saturation
$\underline{Sh}$	Sherwood number
$\overline{Sh_D}$	averaged Sherwood number
T	temperature (K)
V	volume (m^3)
v	velocity ($m\,s^{-1}$)
t	time (s)
t^*	dimensionless purge time
W_{comp}	power required for air compression (W)
w	absolute humidity

Greek letters

α	thermal diffusivity ($m^2\,s^{-1}$)
β	property of diffusion media
Δ	difference
ε	porosity of diffusion media
ρ	density ($kg\,m^{-3}$)
σ	surface tension ($N\,m^{-1}$)
τ	tortuosity
μ	viscosity (Pa s)
φ	relative humidity
η	compressor efficiency
κ	ratio of specific heats
ψ	volume fraction in DM

Subscripts

a	air
avg	average
cap	capillary
CH	channel
cond	conduction
conv	convection
CR	critical condition
CW	channel wall
DM	diffusion media
dry	dry
eff	effective
evp	evaporation
in	inlet
l	liquid water
out	outlet
purge	purge
ref	reference
s	surface
trans	transport
w	water
wet	wet
0	main body of test rig channel
1	top surface of DM
2	bottom surface of DM
∞	bulk stream

Extensive research of evaporation from porous media can be found in petroleum and civil engineering. Kaviany et al. investigated the drying of porous media utilizing non-hygroscopic granular beds with experimental and analytical approaches [13,14]. Water movement and distribution in porous media during evaporation were investigated with nuclear magnetic resonance (NMR) [15], refractive index [16], and neutron radiography [17] to understand the immiscible displacement of water. Some fundamental understanding of drying was achieved through pore network modeling, in which effects of microstructure of pore on drying mechanism, water movement and redistribution were analyzed [18–21]. However, most studies were focused on evaporation from purely hydrophilic media with fixed flow rate of purge gas, which is quite unlike normal PEFC DM. Recently, Shahidzadeh-Bonn et al. performed experimental study on the impact of wetting properties on the kinetics of drying of porous media [22]. However, the effect of surface property was investigated only for pure hydrophilic or pure hydrophobic porous media, respectively. Therefore, the effects of flow rate of purge gas on porous media with mixed wettability similar to fuel cell DM were not evaluated.

The influence of DM properties on water removal and retention was recently conducted in an *ex situ* environment [23]. However, a specific investigation of the DM by itself to clarify and understand the fundamental behavior is still needed.

Slow evaporation experiments have been fully performed in soil science area to understand the physics of water movement in pores during evaporation. However, it has been challenging to apply the method into DM for PEFC due to the thinness of DM and limitations of experiment. The motivation of the study is the need to reduce the parasitic losses necessary to purge the fuel cell and reduce the potential for damage at shutdown. To help achieve this, the objective of this study is to investigate the fundamental behavior of evaporative water removal from fuel cell diffusion media with a special test rig developed to minimize in-plane gradients so that through-plane evaporative behavior can be analyzed. In this paper, new test methods are introduced to understand behavior of water evaporation from DM, and effects of external boundary condition were investigated for the first time. From fundamental understanding of physics underlying the evaporation, critical relations for designing optimal gas purge were developed.

2. Experimental

2.1. Artificial saturation of DM

Diffusion media were saturated with de-ionized (DI) water by immersion in DI water contained in transparent plastic cylinders, and then depressurized to 26 cmHg by vacuum pump (WELCH™ Model 25618-50). Through the pressure difference developed between air in the pores and DI water, along with frequent vibra-

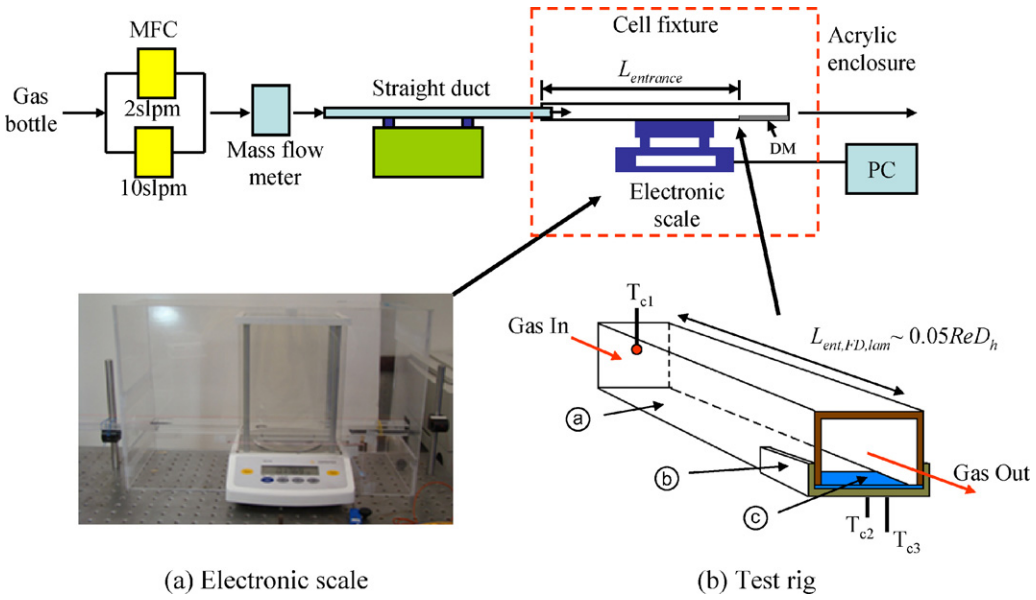

Fig. 1. Schematic of the evaporation test setup: (a) electronic scale and (b) test rig.

tion, the DI water was fully imbibed into the pores in DM. It should be noted that to facilitate examination of the evaporative behavior of the media under a wide range of saturation, the media were initially saturated to higher values (0.5–1.0) of saturation than are typical in PEFCs. Based on previous studies using neutron imaging [11], the normal range of saturation in the DM in operating cells is around 0–0.3.

2.2. Determination of initial saturation of DM

At shutdown, depending on the operating history, water can remain at different saturation levels in DM. Therefore, the effect of initial residual water saturation in DM was investigated by utilizing the artificial saturation method with vacuum pump previously described. The DM were slightly oversaturated with DI water, and installed in the evaporation test rig. By applying dry air at very slow rate (less than 0.1 SLPM) into the top surface of wet DM, the weight decreased to the point at which the DM had an amount of water equivalent to the desired initial saturation of DM, as calculated below.

$$\text{Saturation } (s) = \frac{\text{Pore volume filled with liquidwater}}{\text{Total dry pore volume of DM}} = \frac{(m_{wet,DM} - m_{dry,DM})/\rho_w}{\varepsilon V_{DM}} \quad (1)$$

where $m_{wet,DM}$ is weight of wet DM, $m_{dry,DM}$ is weight of dry DM, ρ_w is density of water, ε is porosity of DM, and V_{DM} is volume of DM.

When saturation of DM approached 20% more than the desired saturation level, the air supply was stopped, and the remaining water was removed by vapor diffusion. Water content decreased at very slow rate, typically reaching the desired saturation level in about 30 min. By performing this treatment, temperature and water before initiating the experiment could be assumed to be uniformly redistributed in DM [14,29].

2.3. Evaporation test setup

A test rig was developed for directly measuring the evaporative water removal rate of DM, as shown in Fig. 1. The main objective in the design was to facilitate understanding and analysis of the fundamental evaporation from the diffusion media, thus, all in-plane gradients were minimized while maintaining a fully developed hydrodynamic and thermal boundary layer over the sample. The flow rate of purge gas was controlled by two mass flow controllers (MKS™ mass flow controllers, 2 SLPM (standard liter per minute at 0 °C and 1 atm) and 10 SLPM, respectively), and monitored with two flow meters (Omega™ mass flow meter, 2 SLPM and 10 SLPM, respectively).

The test rig consists of a straight channel (ⓐ) and a sample holding plate (ⓑ) to investigate gas purge in stream-wise direction of fuel cell, as shown in Fig. 1(b). Acrylic material was utilized for the cell fixture due to its transparency and low density. The channel (ⓐ) is 15 mm in depth and 25 mm in width, and the depth-to-width ratio of 0.6 simulates a typical flow field design. The hydraulic entrance length is 350 mm, which is enough to achieve the fully developed laminar flow condition up to a Reynolds number of 370 (7 SLPM). In the experiments conducted, flow rate was varied in the range of 0.25 SLPM to 7 SLPM. *Therefore, a fully developed laminar condition at the leading edge of the DM sample was achieved for all test conditions*. The results of this study are therefore applicable for laminar flow regimes, and additionally study would be needed to assess the impact of turbulent flow. However, in an actual fuel cell stack, the purge flow rate does not normally exceed the flow rate needed for the maximum operation condition (generally less than 1.5 A cm^{-2}), and the maximum flow rate for purge is therefore within the laminar range in the flow field. Based on the actual gas flow rate used in stacks, and actual channel geometries that are typical, a flow rate in this range was decided (for example, the 7 SLPM is equivalent to gas flow rate (Reynolds number) needed for operation at 1.5 A cm^{-2}).

The end region of the channel (ⓐ) has an open bottom side, to which a DM (ⓒ) was applied with a sample holding plate (ⓑ). In order to reduce the wetting effects on interfaces between water in bottom of DM and top surface of sample holder, a hydrophobic DuPont™ Teflon® sheet was applied onto the top surface of sample holder. The inside and bottom of the channel (ⓐ) which contacts with DM was also coated with Dupont™ Teflon wax, and dried at room temperature for 1 h before start of experiment to reduce any possible wetting between cell channel and water in DM.

As described in Fig. 1(b), the DM was fixed in its position with the cell fixture by an elastic band at the very low compression pressure of 0.13 psi, and the DM was maintained as flat during evaporation.

Compression of 3 mm width of DM (10.7% of total DM) is assumed to have a negligible effect on the total evaporation behavior of DM with an uncompressed 25 mm width (89.3% of total DM) due to the negligible compression of DM and wetting effect between DM and the channel, and high in-plane permeability of DM. Temperature change of DM was measured in separate tests under identical experimental conditions. As described in Fig. 1(b), the temperature of inlet purge gas and two locations of DM (5 mm and 45 mm apart from leading edge, respectively) were measured with thermocouples (OMEGA® T-type thermocouple).

For testing, DM of SGL™ Sigracet® 10 series (10AC) with dimensions of 28 mm width and 50 mm length were utilized. This width enabled an accurate weight change measurement with small error while being short enough to minimize any in-plane temperature, saturation, or vapor pressure gradients that would cause a smearing in the results, and make any interpretation more difficult. 10AC is porous carbon-felt structure with micro-porous layer (MPL) on one side, and in experiment, the MPL side was positioned on to the sample holder, and top surface of the macro-porous layer of DM was exposed to the purge gas to investigate water removal behavior from the macro-porous layer. From extensive testing with different sample lengths of DM, 50 mm was determined to be the proper sample length to ensure near uniform boundary conditions. Use of a longer sample is inappropriate for this measurement, since the leading edge of the sample would face very different boundary and internal saturation conditions than the trailing edge. In a full-size fuel cell, the DM will experience a full range of saturations and boundary conditions during purge. The results here can be easily applied to understand and predict the evaporative removal along the channel during purge with a discretized control volume approach.

As shown in Fig. 1(a), the weight change of DM during evaporation was measured with a precise electronic scale (Satorius™ Model TE214S) with maximum capacity of 210 g and accuracy of ±0.1 mg. Weight changes were recorded at 0.2 s intervals. For the single layer of DM utilized in the experiment, the total weight of water saturated in the DM is about 416 mg when fully saturated. Therefore, the scale can be utilized with a maximum error of ±1%, even down to a low saturation level of 0.02. It is important to note that in the tests performed, the tests were conducted until the sample was fully dry. In practice, this is not necessary, would take an excessive amount of energy, and would also over-dry the membrane. The tests conducted here were continued until full dry out because the main objective was to understand the fundamental nature of the evaporation throughout the entire potential saturation range.

The room temperature was controlled to be 26 °C within +0.4 °C, and relative humidity was maintained between 35% and 40% at room temperature conditions. Evaporation testing was conducted more than three times for each test condition, and data were averaged for analysis. The maximum deviation between recorded data was ±1.5% for the range of moderate saturation level of DM from 0.5 to 0.1, and ±5.8% for lower saturation level of 0.02. This represents a satisfactory level of repeatability for the tests conducted.

3. Results and discussion

3.1. Characteristic modes of water transport during purge

Water removal from a saturated DM is characterized by three distinct regimes, as illustrated in Fig. 2; a surface evaporation regime (SER), a constant rate period (CRP) regime, and finally a falling rate period (FRP) regime. The regime characteristics are controlled by the combined effects of evaporation at the open surface of DM and liquid water transport through DM by capillary action.

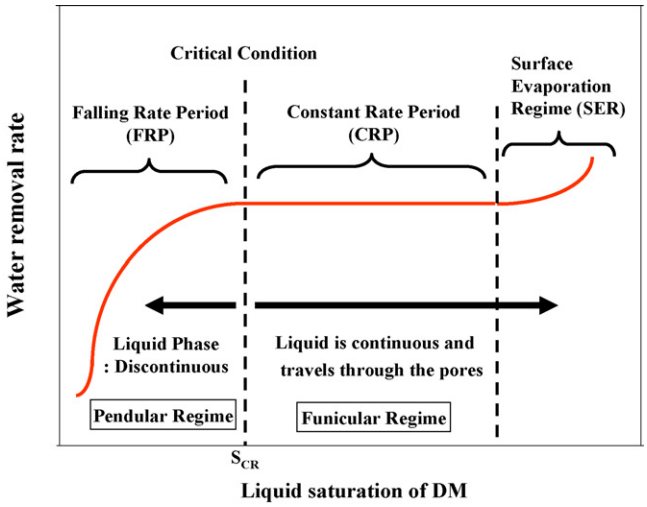

Fig. 2. Characteristic evaporative water removal curve of DM.

Thermodynamically, water evaporation at the surface is controlled by a vapor concentration gradient between surface and bulk flow of purge gas, as described in Eq. (2). The evaporation rate is a function of Reynolds number (Re) and Schmidt number (Sc) of the purge gas [24]. Those parameters can be represented by the average Sherwood number ($\overline{Sh}$) [25]. Therefore, the theoretical evaporation rate can be related with $\overline{Sh}$

$$\begin{aligned} \dot{m}_{w,evp} &= \overline{h_m} A_{s,DM}(\rho_{w,s} - \rho_{w,\infty}) \\ &\sim f(Re, Sc) \sim f(\overline{Sh}) \end{aligned} \quad (2)$$

where $\dot{m}_{w,evp}$ is water evaporation rate, $\overline{h_m}$ is the average mass transfer coefficient, $A_{s,DM}$ is surface area of DM exposed to flow, $\rho_{w,s}$ is saturated water vapor density on the surface of DM, $\rho_{w,\infty}$ is water vapor density in bulk air stream. Note that this does not take into account surface effects, which can play a role in the phase change process, but are not believed to be rate limiting in this case.

The motion of liquid water in the DM is governed by gravity, capillary, and thermo-capillary forces. Moreover, under isothermal conditions and with negligible gravity impact (as can be shown to be true in a fuel cell DM under normal conditions [26]), capillary liquid transport is dominant, which can be described by Darcy's equation. The liquid flow (i.e. capillary-driven flow) is controlled by structure of DM such as pore diameter (d), porosity (ε), permeability (K), tortuosity (τ) as usually, surface properties of the DM including surface tension (σ), capillary pressure (P_C), and saturation (s). Those parameters can be grouped functionally into property of DM (β) and saturation level of DM (s), and finally liquid water transport can be described in a functional relation with β and s:

$$\begin{aligned} \dot{m}_{w,trans} &\approx \dot{m}_{w,cap} = -\frac{\rho_w k_w}{\mu_w}\nabla P = -\frac{\rho_w K}{\mu_w} k_r \left(\frac{dP_C}{ds}\right)\nabla s \\ &\sim f[(d, \varepsilon, K, \tau), s(\sigma, P_C)] \\ &\approx f(\beta, s) \end{aligned} \quad (3)$$

where $\dot{m}_{w,trans}$ is liquid water transport rate in the DM, $\dot{m}_{w,cap}$ is capillary flow rate of liquid water, ρ_w is density of liquid water, k_w is permeability of liquid water in the DM, μ_w is viscosity of liquid water, K is absolute permeability of the DM, and k_r is the relative permeability of the DM.

Water removal from the DM can be characterized as a function of surface evaporation and liquid water transport through DM, and it can be simplified as function of Sherwood number ($\overline{Sh}$) and saturation of DM (s) for a prescribed DM. From those relations, purge

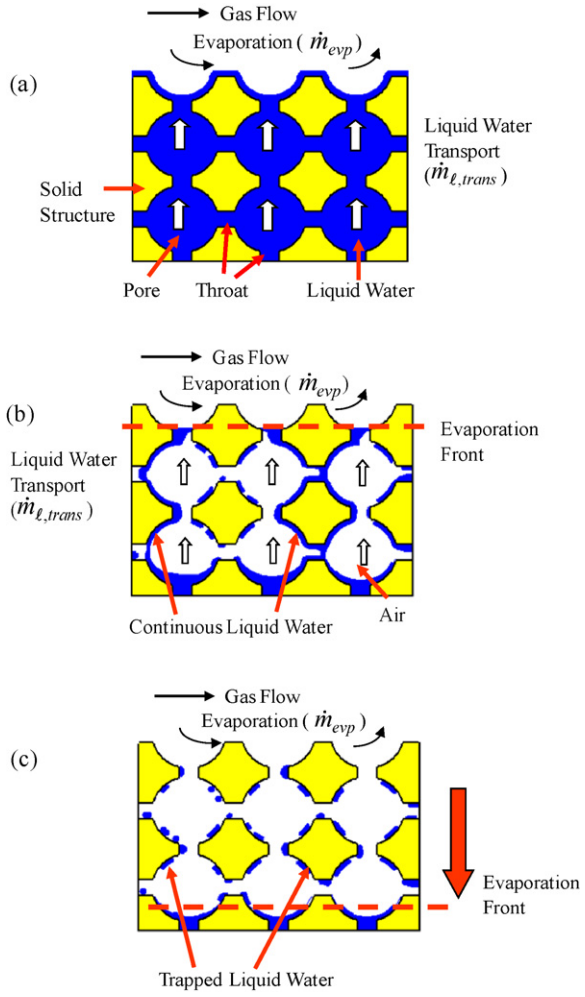

Fig. 3. Schematic description of water transport modes in DM during gas purge in idealized structure: (a) water removal at SER and CRP regimes ($\dot{m}_{l,trans} > \dot{m}_{w,evp}$), (b) water removal at critical condition ($\dot{m}_{l,trans} = \dot{m}_{w,evp}$), and (c) water removal in FRP regime ($\dot{m}_{i,tran} < \dot{m}_{w,evp}$).

time can be correlated with $\overline{Sh}$:

$$\begin{aligned} \dot{m}_{w,rem} &\sim ds/dt \\ &\sim f(\dot{m}_{w,evp}, \dot{m}_{w,cap}) \\ &\sim f(\overline{Sh}, \beta, s) \approx f(\overline{Sh}, s) \end{aligned} \quad (4)$$

$$t_{purge} \sim f(\overline{Sh}) \quad (5)$$

where $\dot{m}_{w,rem}$ is water removal rate, and t_{purge} is purge time.

From this, it is expected that evaporative water removal for a prescribed DM can be correlated for purge time and various purge conditions, as will be shown in the following sections.

3.2. Characteristic water removal curve of DM

When purge gas is supplied to a saturated DM, water residing near the surface is initially rapidly removed. This behavior of water removal is shown as the surface evaporation regime (SER) in Fig. 2 which illustrates a typical water removal behavior versus saturation of DM. After this, water is removed from main body of DM, balanced with internal flow of liquid water to the evaporating surface. In this regime, liquid transport is a result of capillary flow via hydraulic connections among pores, and it is rapid enough to balance the rate of water removal at surface, as illustrated in Fig. 3(a). Therefore, a constant water removal rate period (CRP) is achieved. This level can be thought of as a maximum sustainable level of water removal achievable for a given material, and serves as a useful guideline to compare internal capillary flow rates between different DM designs. This regime of internally connected capillary liquid flow is known as the funicular regime [13,14,27]. As purge proceeds further, the saturation decreases, and the hydraulic connections between residual liquid diminish, causing the rate of water displacement to be decreased. Eventually, the maximum capillary supply rate is equal to the rate of water removal, as shown in Fig. 3(b). This is termed the critical condition. As purge is continued, more hydraulic connections are broken, and separated liquid water droplets are trapped inside of pores as droplets. This is known as the pendular regime [13,14,27], and further saturation reduction must be achieved by vapor diffusion. As described in Fig. 3(c), after this critical point, liquid water cannot be transported to the dry front by capillary action any further, and therefore the evaporation front starts to penetrate into DM to evaporate water droplets trapped in pores, causing the rate of water removal to significantly decrease. This behavior is known as falling rate period (FRP) regime in Fig. 2. From transition between funicular regime and pendular regime, irreducible saturation can be obtained. A detailed description of the characteristics of evaporation and two phase regimes can be found in refs [13,14,18–21,27–29]. It should be noted that water removal rate decreases significantly after the critical point, and as a practical consequence, purge becomes less efficient beyond this point. Therefore, the critical condition can be utilized as a baseline for analyzing evaporative purge efficiently between water removals.

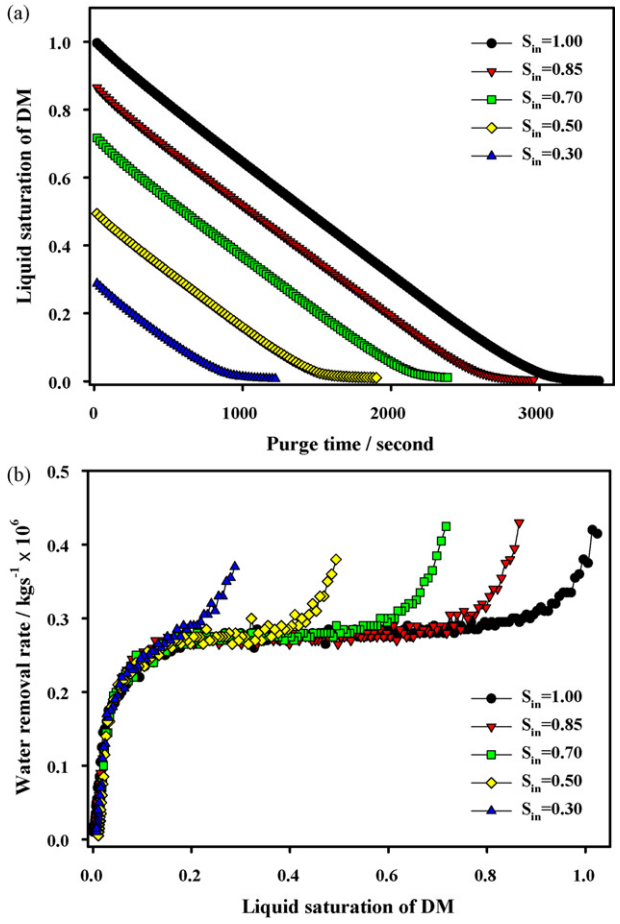

Fig. 4. Water removal behavior for different initial content of water in the DM (28 mm × 100 mm) at purge gas flow rate of 7 SLPM: (a) variation of water amount (saturation) in DM during gas purge and (b) variation of water removal rate with respect to initial saturation of DM.

3.3. Impact of initial saturation level on characteristic results

Results for tests conducted with a range of initial saturation during gas purge were shown in Fig. 4(a). In order to understand the transient water removal behavior, the test results were converted to water removal rate, and compared with respect to saturation of DM in Fig. 4(b). Evaporation curves for each condition of initial saturation showed the three distinct evaporation regimes described in previous section. The CRP and FRP overlapped for each initial saturation condition, and the only difference was the duration of CRP was different. The consistent and reliable results for each condition indicate temperature and water in DM were almost uniformly distributed before start-up of gas purge for each case. Because all three regimes of evaporative removal could be simulated, and DM are generally less than 50% saturated with water in actual fuel cell operation [11], an initial saturation of 50% was determined to be the baseline for further testing.

3.4. Impact of purge flow rate on water removal

Water removal behavior was investigated with dry air as a purge gas at room temperature at flow rates from 0.25 SLPM to 7 SLPM. The measured water removal rate was compared with respect to purge time, as shown in Fig. 5(a). The critical condition was obtained more rapidly with higher flow rate, and therefore efficient purge seems to be achieved with higher flow rate of purge. However, the resulting residual saturation at the critical time is greater than that at low flow rate. Depending on the desired final saturation levels (generally, a slight drying of the membrane is desired but incomplete dry out of the DM is acceptable), it might be beneficial to use a lower flow rate (and lower energy) purge to achieve a reduced

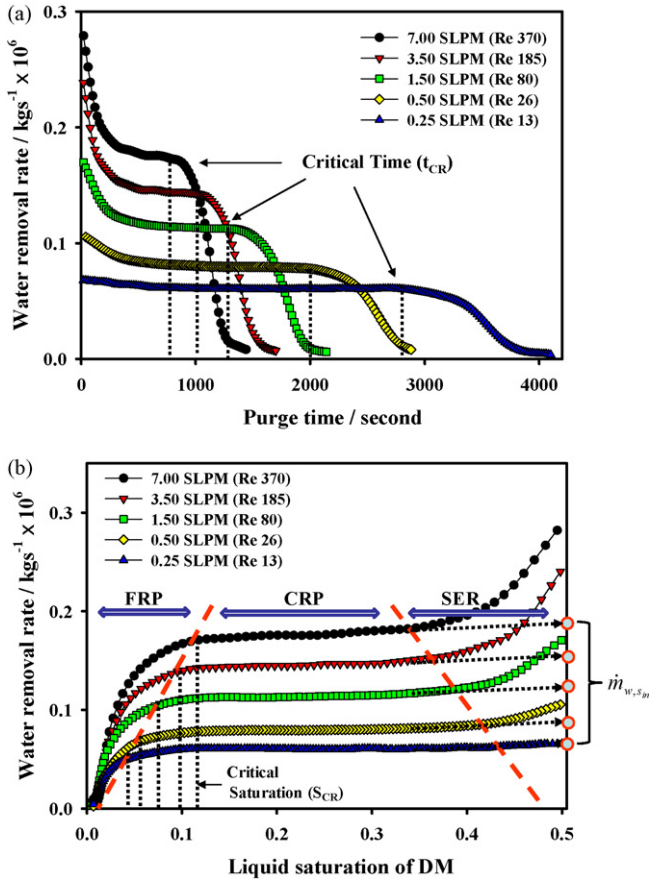

Fig. 5. Comparison of water removal rate during gas purge: (a) with respect to purge time and (b) with respect to saturation.

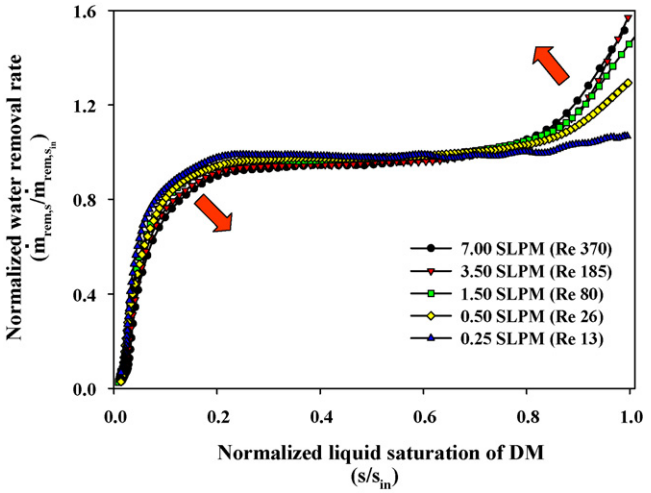

Fig. 6. Effect of flow rate of purge gas on water removal rate: comparison of water removal behavior in normalized plot.

saturation level. That is, the fastest flow rate is not necessarily the best choice to achieve low saturation.

Effect of flow rate on water removal was further compared with respect to relative humidity of the exit purge gas. The relative humidity of the exit purge gas was found to increase from 7% to 50% in the CRP regime as flow rate decreased from 7 SLPM to 0.5 SLPM. Detailed calculation of relative humidity of exit purge gas was described in Appendix C.

By using Eq. (1), the water amount in DM was converted to liquid saturation of DM, as shown in Fig. 5(b). The expected three characteristic regions of water removal were obtained with respect to saturation and purge flow rate. For higher flow rate of purge, the range of saturation for CRP regime is reduced, and the critical condition of transition between constant and falling evaporation rate regimes was obtained at higher residual saturation (i.e. higher content of water is left after the transition to a FRP at that flow rate) in DM. A lower flow rate purge extended the saturation range for CRP to a lower transition saturation, and the critical condition was obtained at a reduced saturation. *Therefore, although a high flow rate of purge can rapidly reach a critical time, a greater liquid saturation remains in DM after the critical point. Additionally, doubling the flow rate does not half the time required to reach a specific saturation value.*

3.5. Mechanism of effect of flow rate on water removal

The water removal rate as a function of flow rate was calculated and is shown in Fig. 6. Normalization was achieved by dividing water removal rate during purge with water removal rate obtained by extrapolating the tangent lines from CRP to initial saturation, as shown in Fig. 5(b). Water removal in the SER increased significantly with flow rate. In this regime, evaporation is mainly conducted on the liquid water residing on the open surface of DM, and therefore, much larger surface area of the water can be invaded by purge gas, leading to the very fast water removal and sensitivity to flow rate. When evaporation starts in the CRP regime, the surface area of liquid exposed to purge gas is varied by combined effects of open boundary and liquid water supply to the drying front. For low flow rate of purge, the surface area of water exposed to purge gas is maintained due to the rapid capillary flow rate to the evaporating surface. However, for a higher purge flow rate, the surface area can be reduced due to higher evaporation rate at the open boundary. Those effects of surface area variation on water removal rate can be observed in Fig. 6, where CRP regime slightly deviated from the expected plateau for higher flow rate.

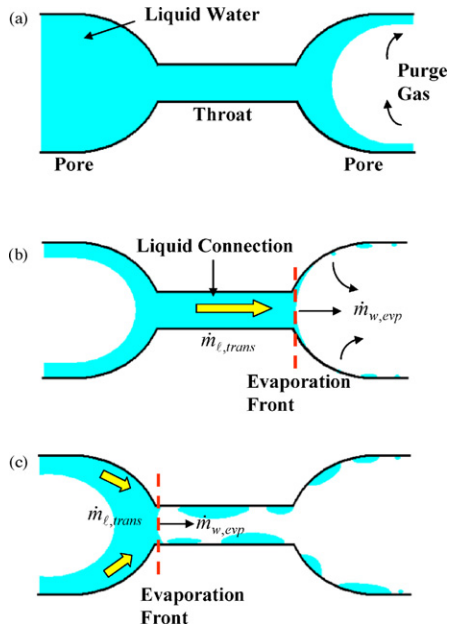

Fig. 7. Schematic description of water removal from DM for different flow rates of purge gas: (a) before gas purge, (b) for slow flow rate of purge gas, and (c) for fast flow rate of purge gas.

Another characteristic effect of flow rate was found in the transition from CRP to FRP. As discussed, the transition from CRP to FRP was generated at higher saturation level of DM for a higher flow rate of purge gas. This can be explained by considering the concept of hydraulic connectivity through pores. When a slow flow rate of purge gas is applied, evaporation rate is slow, and therefore capillary liquid transport in DM can readily balance the evaporation in the open boundary and still maintain a hydraulic connection between pores until a lower DM saturation as illustrated in Fig. 7(b). Therefore, the transition to FRP is generated at a lower saturation level for a lower flow rate purge.

However, when the purge flow rate is very high, the evaporation rate in the open boundary becomes very rapid, and liquid supply through DM cannot balance the rate of evaporation, even when DM has a higher saturation. Therefore, the evaporation front starts to penetrate into pores, resulting in sudden drop of water removal rate, as illustrated in Fig. 7(c). As a result, the transition is generated at higher saturation level for higher flow rate of purge gas. Vapor diffusion in DM is another mode of water removal, but due to the low water removal rate, it is only a dominant mode in the FRP regime, where capillary liquid transport does not exist.

3.6. Thermal analysis and empirical relation

Drying involves phase change from liquid to vapor phase, and energy is required for the phase change. The coupled effects of heat and mass transfer were investigated by measuring temperature variation of the DM during purge. Due to the experimental limitations, temperature measurement of DM could not be simultaneously conducted with weight change measurement. In order to precisely measure the water variation in the DM, the test fixture on the electronic scale should be stand-alone, mechanically isolated from other components. When thermocouples are utilized during evaporation, the thermocouples applied to the test rig are connected to thermometer by the sensing cables to monitor and record the temperature variation, leading to inaccurate weight change measurement. Therefore, temperature measurement was conducted separately, but under identical experimental conditions. Temperatures of inlet purge gas and two locations of DM (5 mm and 45 mm apart from leading edge, respectively) were measured with thermocouples, as shown in Fig. 1(b).

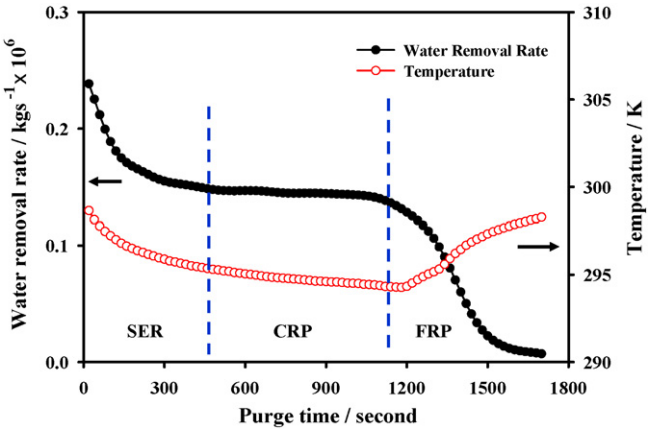

Fig. 8. Temperature variation of DM during gas purge at 3.5 SLPM.

As shown in Fig. 8, the temperature of DM varied in a similar manner to that of water removal rate, as expected. Temperature decreased in the SER regime due to rapid evaporation of water, and then decreased steadily in the CRP regime. As purge further proceeded, water removal by evaporation was decreased, and evaporative heat loss becomes lower than the heat supply into the DM, causing the temperature of the DM to increase back to the ambient conditions. Temperature was decreased by a maximum of −5.5 °C for 7 SLPM, −4.7 °C for 1.5 SLPM, and −4 °C for 0.5 SLPM. The temperature difference between TC_2 and TC_3 in Fig. 1(b) was measured to be less than 0.8 °C, even at the most severe condition of the highest flow rate of purge. Therefore, the in-plane direction of DM during the purge experiments can be considered to be nearly isothermal, which is consentient with the desire to minimize in-plane gradients that can make interpretation of the results difficult. The through-plane temperature difference can be assumed to be negligible due to the thinness and high thermal conductivity of DM. This assumption can be easily verified, as addressed in Appendix A. Therefore, although the DM temperature changes during the experiment, it can be considered as spatially uniform in temperature. Heat transfer due to conduction from the channel wall can be assumed to be negligible, and the heat loss due to evaporation can be related solely with convection heat from air stream, as described in Appendix B.

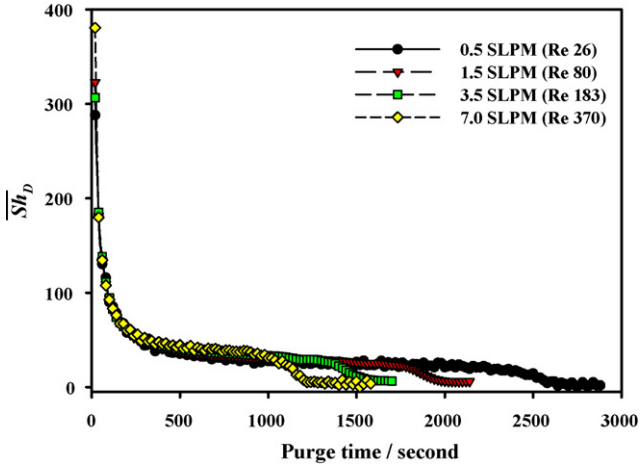

Fig. 9. Variation of Sherwood number ($\overline{Sh}_D$) during gas purge.

Table 1
Material and transport properties.

Description	Unit	Value
Binary diffusion coefficient of water to air at 298 K and 1 atm[a] [32]	$m^2\ s^{-1}$	0.26×10^{-4}
Density of air at 298 K and 1 atm[a] [25]	$kg\ m^{-3}$	1.17
Density of water at 298 K and 1 atm [25]	$kg\ m^{-3}$	997.10
Heat capacitance of air at 298 K and 1 atm[a] [25]	$kJ\ kg^{-1}\ K^{-1}$	1.00
Heat capacitance of water at 298 K and 1 atm [25]	$kJ\ kg^{-1}\ K^{-1}$	4.18
Hydraulic diameter	m	18.75×10^{-3}
Latent heat of evaporation of liquid water at 298 K and 1 atm[a] [25]	$kJ\ kg^{-1}$	2442.30
Length of cell fixture channel	m	0.45
Porosity of DM [28]	–	$0.82 \pm 0.5\%$
Surface area of DM (measured)	m^2	1.40×10^{-3}
Thermal conductivity of acrylic material [25]	$W\ m^{-1}\ K^{-1}$	0.2
Thermal conductivity of DM [33]	$W\ m^{-1}\ K^{-1}$	0.48
Thermal conductivity of water at 298 K and 1 atm [25]	$W\ m^{-1}\ K^{-1}$	0.60
Thermal diffusivity at 298 k and 1 atm[a]	$m^2\ s^{-1}$	22.5×10^{-6}
Thickness of diffusion media (measured)	m	$(0.37 \pm 0.01) \times 10^{-3}$
Volume of dry diffusion media (measured)	m^3	$(5.15 \pm 0.14) \times 10^{-7}$
Weight of dry diffusion media (measured)	kg	$(0.19 \pm 0.004) \times 10^{-3}$

[a] In the case of non-isothermal condition, values corresponding to each temperature were applied for calculation.

From analogy between mass and heat transfer [14,25], the mass transfer coefficient can be obtained.

$$\overline{h_m} = \frac{\overline{h_{conv}}}{(\rho c_p)_a Le^{2/3}} \tag{6}$$

where

$$Le = \frac{\alpha_a}{D} \tag{7}$$

$$D(T, P) = D(T_{ref}, P_{ref}) \left(\frac{T}{T_{ref}}\right)^{3/2} \left(\frac{P_{ref}}{P}\right) \tag{8}$$

where $\overline{h_m}$ is average mass transfer coefficient, ρ_a is density of air, $c_{p,a}$ is heat capacity of air, Le is Lewis number, α_a is thermal diffusivity of air, D is binary diffusion coefficient of water into air, T_{ref} is reference temperature (298 K), and P_{ref} is reference pressure (1 atm).

The average Sherwood number ($\overline{Sh_D}$) is calculated as shown below, and the results were plotted in Fig. 9 with respect to purge time. The material and transport properties used for the calculation are described in Table 1.

$$\overline{Sh_D} = \frac{\overline{h_m} D_h}{D} \tag{9}$$

where D_h is hydraulic diameter of test rig channel.

Purge time was normalized with the critical time for each flow rate, and compared with $\overline{Sh_D}$ in the log–log plot of Fig. 10(a). $\overline{Sh_D}$ was found to be clearly related with normalized time for each flow rate condition. By normalizing with Re^n, all the relations of $\overline{Sh_D}$ for each flow rate collapsed into a characteristic purge curve in Fig. 10(b), where n was found to be 0.2 from regression analysis.

$$\log\left(\frac{\overline{Sh_D}}{Re^{0.2}}\right) = 0.19(t^{*2} - 1.2t^* + 5.6) \qquad R^2 = 0.99 \tag{10}$$

where t^* is $\log(t/t_{CR})$.

It should be noted that water removal during gas purge decreases significantly at the critical condition, and purge effectiveness decreases substantially. Therefore, gas purge is most efficient if terminated at the critical condition, and a quantified relation for gas purge until onset of critical condition is needed. An empirical relation was developed for the regions from initial purge to onset of the critical condition. This equation is a characteristic relation between evaporative water removal rate and purge time for SGL 10 series DM (10AC), and can be generally utilized for other purge conditions for this material even though it was developed from purge gas of dry air and room temperature, because the right hand side of Eq. (11) has terms normalizing the effect of different type of purge gas, flow rate, relative humidity and temperature.

$$\overline{Sh_D} = \frac{\overline{\dot{m}}_{w,evp}}{D(\rho_{w,s} - \rho_{w,\infty})} \tag{11}$$

$$Re = \frac{\rho v D_h}{\mu} \tag{12}$$

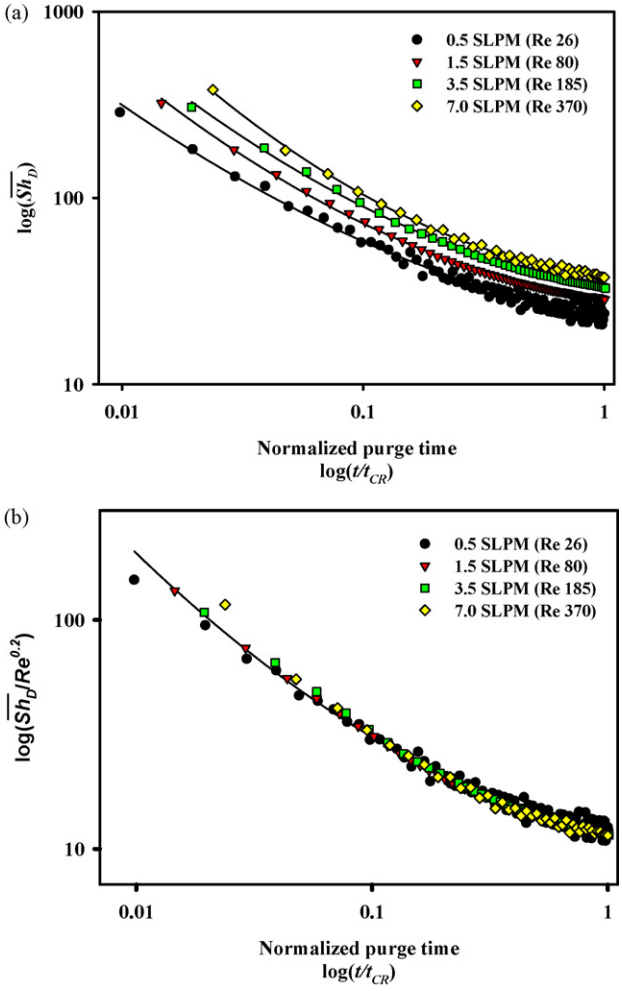

Fig. 10. Correlation of Sherwood number ($\overline{Sh_D}$) with purge time: (a) variation of $\overline{Sh_D}$ for each flow rate and (b) normalization of $\overline{Sh_D}$ with Re^n.

where $\overline{m}_{w,evp}$ is average water evaporation rate, *Re* is Reynolds number, ν is velocity of purge gas, μ is viscosity of purge gas.

However, there are some limitations for application of this relation. The relation is valid only for the continuous liquid-phase regime (from initial purge to critical condition), and therefore for the conditions beyond this regime such as the pendular regime, or temperature above boiling point of water and temperature below freezing point of water, the relation is not applicable. This result is appropriate unless other parametric effects not studied in this paper dominate mass transport and water removal from the DM. Notably, in full size cells temperature gradients can be established that significantly impact total evaporative removal rates. Additionally, the effect of land/channel structure of the flow field was not considered in this study, as the purpose of this study is to understand the evaporative water removal behavior of DM itself. Further variation of the system setup to simulate a channel/land structure can be achieved with some modifications to the sample holder, which will be a topic for the future study.

Attempts at obtaining a similar relationship for evaporation behavior in the falling rate (pendular) regime were unsuccessful, perhaps due to the multiple regressing evaporation plane locations at the droplet surfaces in the saturated media.

3.7. Purge efficiency

The impact of purge flow rate on purge efficiency was previously discussed with respect to purge time and content of water remained in DM at the critical condition. However, for determining optimal purge protocol, total energy requirement should also be considered. The energy requirement for purge was calculated for the cell fixture used in this study as a qualitative guideline. Detailed equations utilized for calculation of energy are described in Appendix D.

As described in Fig. 11, when higher flow rate of purge was applied, the critical condition was obtained more rapidly, however the residual saturation in the DM was larger and more energy was required to achieve the critical condition. Whereas, for the lower flow rate, the energy requirement and water remained in DM were lower, although longer purge time was needed to achieve the critical condition. Fig. 11 can be used as a guideline for determining proper purge condition according to individual system requirements.

3.8. Purge for enhanced durability

The coupled effects of fuel cell components on evaporative water removal during gas purge were conceptually investigated by comparing the HFR plot available in literature [2] and evaporation curve

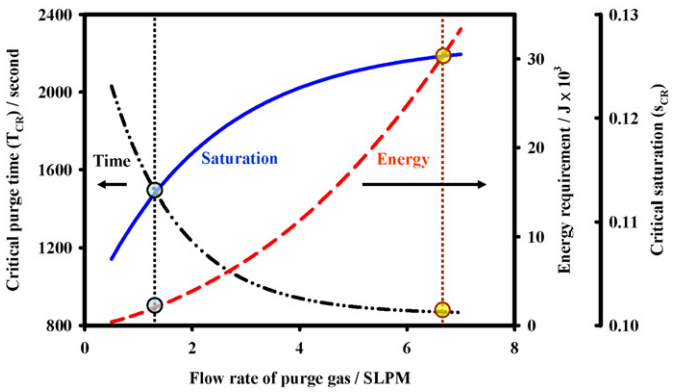

Fig. 11. Effect of purge parameters on efficiency of gas purge.

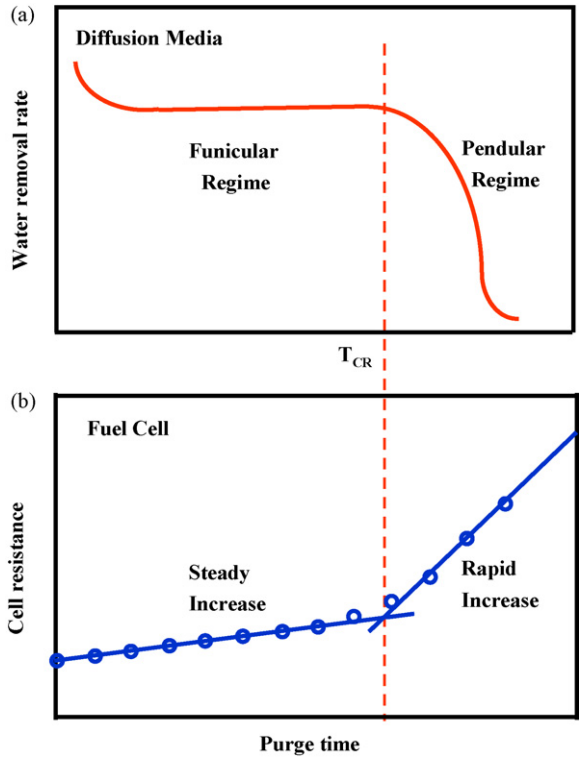

Fig. 12. Conceptual comparison of water removal of DM with HFR variation of fuel cell during gas purge: (a) water removal behavior of DM and (b) HFR variation of fuel cell (redrawn from Ref. [2]).

of DM developed in this study. When gas purge is applied into the fuel cell after shutdown, water is primarily removed from the surface of DM, and then liquid water is supplied from inside the DM and membrane to the evaporating surface, leading to steady increase of HFR due to the gradual decrease of water content in the membrane. As purge further proceeds, the hydraulic connections among pores are broken, and then isolated water is trapped in pores causing the evaporation front to penetrate into DM. Finally, the evaporation front contacts the membrane, and starts to remove water directly from membrane, causing HFR to substantially increase, as shown in Fig. 12(b). Therefore, at the critical condition, water removal rate of DM decreases significantly, resulting in decrease of purge effectiveness, whereas water removal rate from membrane increases substantially, which can result in significant membrane durability issues. Therefore, for efficient and durable purge, most of water should be removed in CRP regime in which water removal is efficient and the evaporation front does not penetrate into the membrane.

Effects of purge flow rate on durability in fuel cell condition can be understood with characteristic water removal behavior of DM to the flow rate of purge. As previously described, for higher flow rate of purge, the purge gas will start to remove water directly from membrane faster, causing HFR to be substantially increased, while the overall saturation in the DM remains higher. This discovery is evidence that the assumption of sequential drying is not proper, and HFR cannot be used to estimate the total water in fuel cell without other diagnostics.

An efficient and durable gas purge can be conceptually described as follows. As shown in Fig. 13, by applying a composite flow rate of purge gas (i.e. a decreasing or staggered flow rate during purge), the maximum amount of water removal can be conducted in the CRP regime, without dry-front penetration to the membrane surface. This composite gas purge can be beneficial in actual fuel cell conditions. Water slugs residing in flow channel or on the DM can be

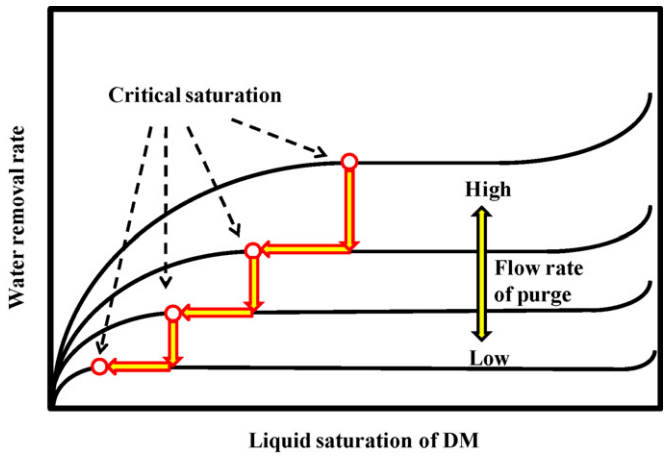

Fig. 13. Conceptual description of efficient and durable purge by utilizing composite flow rate of purge gas.

removed efficiently by short blast purge at high flow rate, and with a gradually decreasing flow rate at critical saturation for each flow rate, the hydraulic connections among pores can be maintained until lowest possible saturation level, providing an efficient purge that reduces membrane moisture gradients that have been shown to negatively impact durability.

4. Conclusions

The objective of this study is to investigate the fundamental behavior of evaporative water removal from fuel cell diffusion media so that ultimately, purge procedures, materials, and design with reduced parasitic losses can be developed. A new test system was developed to directly characterize and compare evaporative water removal from diffusion media (DM) during gas purge with minimal in-plane gradients in saturation, temperature, and vapor pressure for the purpose of fundamental study. From fundamental understanding of evaporative water removal, critical relations for gas purge were obtained. Specifically, the following conclusions are drawn from this study:

(1) The water removal was characterized by three different regimes, a rapid surface evaporation regime (SER), a slower constant rate evaporation period (CRP), and a much slower falling rate evaporation period (FRP) regime.
(2) At the critical condition between CRP and FRP regimes, water removal rate decreased significantly, diminishing purge effectiveness. Therefore, the critical condition is proposed as a key parameter for evaluating purge effectiveness.
(3) An empirical correlation for evaporative water removal was developed for the continuous liquid-phase regime from initial purge to the onset of the critical condition, and relates purge to water removal rate. It can be utilized as a quantitative relation for determining expected water removal rates for the DM tested under high initial saturations.
(4) A generic plot of purge efficiency was developed based on results in this study. It describes the effectiveness of purge parameters including purge time, water saturation in DM, and energy requirement. This relation can be used as a qualitative guideline for designing the overall purge protocol to the requirements of each system.
(5) Purge protocol that enhance durability and reduce parasitic losses were conceptually investigated. For a more durable and efficient purge, most of water should be removed in CRP regime in which water removal is efficient and the evaporation front does not penetrate into the membrane, and it was found to be achieved by applying composite flow rates of purge gas and gradually decreasing flow rate of purge gas at critical saturation for each flow rate to remove most of water in each CRP regime.

The results of this novel study can be applied to larger systems with the expected in-plane temperature, vapor pressure and saturation gradients through computational models to estimate removal times and saturation levels.

Acknowledgments

The authors thank Prof. John Cimbala of Pennsylvania State University for helpful advice, and Dr. B.K. Hong of Hyundai and Kia Motors for providing samples of diffusion media. This work was financially supported by the National Science Foundation (Award CBET-0644811).

Appendix A. Temperature analysis in the through-plane direction of DM

The isothermal assumption in the through-plane direction can be validated considering the extreme condition of heat transfer of DM during evaporation. Heat loss due to evaporation at the surface is assumed as an extreme case to be balanced only by heat supply due to the through-plane temperature difference of DM (i.e. through-plane heat conduction of DM) as described in Eq. (A.1). The variation of effective thermal conductivity of DM ($k_{DM,eff}$) due to water removal in DM is described in volume averaged method as in Eq. (A.2).

$$\frac{\dot{m}_{w,rem}}{A_{s,DM}} h_{\ell g} = k_{t,DM,eff} \frac{T_{DM,2} - T_{DM,1}}{L_{DM}} \tag{A.1}$$

$$k_{t,DM,eff} = (1 - \psi_w) k_{t,DM} + \psi_w k_{t,w} \tag{A.2}$$

$$\psi_w = \frac{V_w}{V_{DM}} \tag{A.3}$$

where $\dot{m}_{w,rem}$ is water removal rate from DM, $A_{s,DM}$ is surface area of DM, $h_{\ell g}$ is latent heat of evaporation of water, $k_{t,DM,eff}$ is effective thermal conductivity of DM, $k_{t,DM}$ is thermal conductivity of DM, $T_{DM,2}$ is temperature of top surface of DM, $T_{DM,1}$ is temperature of bottom surface of DM, L_{DM} is thickness of DM, ψ_w is volume fraction of water, $k_{t,w}$ is thermal conductivity of liquid water, V_w is volume of liquid water, and V_{DM} is volume of DM.

Even in this extreme case, temperature difference of DM between top surface ($T_{DM,1}$) and bottom surface ($T_{DM,2}$) of DM is less than 0.36 °C for the highest flow rate of purge gas. Therefore, in actual cases where heat supply due to forced convection is dominant, the through-plane temperature difference of DM is negligible.

Appendix B. Calculation of heat transfer coefficient

As shown in Fig. 14(a), heat loss due to evaporation is balanced with heat conduction from channel wall of test rig, heat conduction from DM, and heat convection from bulk stream of air. However, the temperature variation of the DM is negligible as described in Appendix A, and therefore conduction heat transfer through DM can be neglected. Therefore, the heat loss due to evaporation is balanced with heat conduction from the channel wall and heat supply by forced convection of air stream. Temperature of the main body of test rig channel ($T_{CW,0}$) is considered to be equal to the room temperature (T_∞), and temperature of the channel wall ($T_{CW,1}$) contacted with DM is assumed to be same as that of DM ($T_{DM,1}$) in Eq. (B.2). The relative magnitude of heat transfer due to conduction by the channel wall to convection by air stream was compared with the ratio of heat transfer, R_q in Eq. (B.5). A maximum average heat

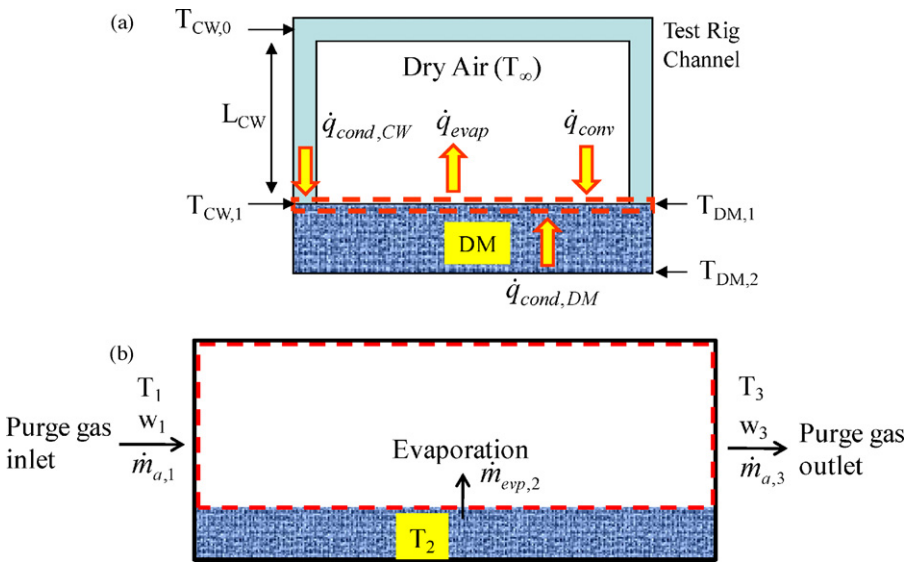

Fig. 14. Schematic description for mass and thermal analysis of DM during evaporation: (a) the front-view image of test rig for analysis of heat fluxes and (b) the side-view image of test rig for calculating humidity of exit purge gas.

transfer coefficient was obtained for the case where heat loss due to evaporation is balanced only by convection heat from purge gas, as shown in Eqs. (B.6) and (B.7). The average heat transfer coefficient was in the range from 570 to 35 $W\,m^{-2}\,K^{-1}$ for the SER and CRP regime, and was minimum 7 $W\,m^{-2}\,K^{-1}$ in FRP regime, which was one to three orders of magnitude greater than heat conduction from the wall of channel, as calculated from Eq. (B.5). Moreover, thermal contact resistance between the tip of channel wall and the surface of DM neglected in the calculation will decrease further conduction heat transfer from channel wall in the actual case. Therefore, heat transfer due to conduction from the channel wall can be assumed to be negligible, and the heat loss due to evaporation was related solely with convection heat from air stream, as shown in Eq. (B.6). And heat transfer coefficient could be calculated from Eq. (B.7).

$$\dot{q}_{cond} + \dot{q}_{conv} = \dot{q}_{evp} \tag{B.1}$$

$$\begin{aligned}\dot{q}_{cond} &= \dot{q}_{cond,CW} + \dot{q}_{cond,DM} \approx \dot{q}_{cond,CW} \\ &= k_{t,CW}\frac{A_{s,CW}}{L_{CW}}(T_{CW,0} - T_{CW,1}) \approx k_{t,CW}\frac{A_{s,CW}}{L_{CW}}(T_\infty - T_{DM,1})\end{aligned} \tag{B.2}$$

$$\dot{q}_{conv} = \overline{h_{conv}}A_{s,DM}(T_\infty - T_{DM,1}) \tag{B.3}$$

$$\dot{q}_{evp} = \dot{m}_{w,rem}h_{\ell g} \tag{B.4}$$

$$R_q = \frac{\dot{q}_{cond}}{\dot{q}_{conv}} = \frac{k_{t,CW}}{\overline{h_{conv}}L_{CW}}\frac{A_{s,CW}}{A_{s,DM}} \approx \frac{7k_{t,CW}}{\overline{h_{conv}}} = \frac{1.4}{\overline{h_{conv}}} \tag{B.5}$$

$$\dot{q}_{conv} = \dot{q}_{evp} \tag{B.6}$$

$$\overline{h_{conv}} = \frac{(\dot{m}_{w,rem}/A_{s,DM})}{(T_\infty - T_{DM,1})}h_{\ell g} \tag{B.7}$$

where $\dot{q}_{cond}$ is heat transferred by conduction, $\dot{q}_{conv}$ is heat transferred by convection, $\dot{q}_{evp}$ is heat loss due to evaporation, $\dot{q}_{cond,CW}$ is heat supplied into DM by conduction from the channel wall of test rig, $\dot{q}_{cond,DM}$ is heat transfer by conduction through DM, $k_{t,CW}$ is thermal conductivity of the channel wall (acrylic material), $A_{s,CW}$ is area of the channel wall contacted with DM, L_{CW} is length of the channel wall, $\overline{h_{conv}}$ is average heat transfer coefficient, $A_{s,DM}$ is surface area of DM, $\dot{m}_{w,rem}$ is water removal rate from DM, $h_{\ell g}$ is latent heat of evaporation of water, and R_q is ratio of heat conduction to heat convection.

Appendix C. Calculation of relative humidity of exit purge gas

Mass balance equations were obtained for the control volume in Fig. 14(b):

$$\text{Air}: \quad \dot{m}_{a1} = \dot{m}_{a3} = \dot{m}_a \tag{C.1}$$

$$\begin{aligned}\text{Water}: \quad &\dot{m}_{w1} + \dot{m}_{evp2} = \dot{m}_{w3} = \dot{m}_a w_3 \\ &\dot{m}_{evp2} = \dot{m}_a w_3\end{aligned} \tag{C.2}$$

where, $\dot{m}_a$ is air flow rate, $\dot{m}_w$ is water vapor flow rate, $\dot{m}_{w1}$ is zero due to dry state of purge gas, $\dot{m}_{evp}$ is water evaporation rate, w is absolute humidity defined with Eq. (C.4), and subscripts 1, 2, and 3 indicate inlet, DM, and outlet region.

Energy balance equations could be obtained for steady state condition:

$$\begin{aligned}&\dot{E}_{in} = \dot{E}_{out} \\ &\dot{m}_a h_1 + \dot{m}_{evp}h_{\ell g2} = \dot{m}_a h_3 \\ &h_1 + w_3 h_{\ell g2} = h_3 \\ &(c_p T_1 + w_1 h_{g1}) + w_3 h_{\ell g2} = c_p T_3 + w_3 h_{g3}\end{aligned} \tag{C.3}$$

where $\dot{E}$ is heat flux, $h_{\ell g}$ is phase change enthalpy from liquid to vapor, c_p is heat capacity of air, T is temperature, and h_g is enthalpy of saturated vapor defined by Eq. (C.5) [34].

$$w_3 = \frac{m_v}{m_a} = \left[\frac{\text{Water removal rate}}{\text{Air supplying rate}}\right] \tag{C.4}$$

$$h_{g3} = 2501.3 + 1.82T_3 \tag{C.5}$$

From the relations, temperature and relative humidity of exit air can be calculated:

$$T_3 = \frac{1}{c_p + 1.82w_3}(c_p T_1 + w_3 h_{\ell g2} - 2501.3w_3) \tag{C.6}$$

$$P_{sat}(T_3) = \exp\left(11.6832 - \frac{3816.44}{T_3 - 46.13}\right) \times 100 \tag{C.7}$$

$$\phi(RH) = \frac{w_3 P_3}{(0.622 + w_3)P_{sat}(T_3)} \tag{C.8}$$

Appendix D. Calculation of power requirement for air compression

The power requirement for air compression was calculated in Eqs. (D.1)–(D.3) [30,31].

$$W_{comp} = \frac{\dot{m}_{a,in} c_{p,a} T_{in}}{\eta_{comp}} \left[\left(\frac{P_{out}}{P_{in}} \right)^{\frac{k-1}{k}} - 1 \right] \quad \text{(D.1)}$$

$$\Delta P = f \frac{L_{CH}}{D_h} \frac{\rho_a v_{a,avg}^2}{2} \quad \text{(D.2)}$$

$$f = \frac{64}{Re} \quad \text{(D.3)}$$

where W_{comp} is power required for adiabatic air compression, $\dot{m}_{a,in}$ is flow rate of purge air, $c_{p,a}$ is the specific heat of air, T_{in} is temperature before compression, P_{in} is pressure before compression, P_{out} is pressure after compression, η_{comp} is compressor efficiency (0.7 was applied here), k is the ratio of specific heats, ΔP is pressure difference between P_{out} and P_{in}, f is friction factor, L_{CH} is length of channel, D_h is hydraulic diameter of channel, ρ_a is density of air, and $v_{a,avg}$ is average velocity of air.

References

[1] S. Kim, M.M. Mench, J. Power Sources 174 (2007) 206–220.
[2] J. St-Pierre, J. Roberts, K. Colbow, S. Campbell, A. Nelson, J. New Mater. Electrochem. Syst. 8 (2005) 163–176.
[3] P.K. Sinha, C.-Y. Wang, J. Electrochem. Soc. 154 (2007) B1158–B1166.
[4] K. Tajiri, C.-Y. Wang, Y. Tabuchi, Electrochim. Acta 53 (2008) 6337–6343.
[5] R. Fuss, US. Patent 6,358,637B1 (2002).
[6] R. Bradean, H. Haas, K. Eggen, C. Richards, T. Vrba, ECS Trans. 3 (2006) 1159–1168.
[7] S. Kim, M.M. Mench, J. Electrochem. Soc. 156 (2009) B353–B362.
[8] K.T. Cho, A. Turhan, J.H. Lee, J.S. Brenizer, A.K. Heller, L. Shi, M.M. Mench, Nucl. Instrum. Methods Phys. Res. Sect. A 605 (2009) 119–122.
[9] D.L. Wood, J.S. Yi, T.V. Nguyen, Electrochim. Acta 43 (1998) 3795–3809.
[10] F.Y. Zhang, X.G. Yang, C.Y. Wang, J. Electrochem. Soc. 153 (2006) A225–A232.
[11] A. Turhan, K. Heller, J.S. Brenizer, M.M. Mench, J. Power Sources 180 (2008) 773–783.
[12] S. Ge, C.-Y. Wang, Electrochim. Acta 52 (2007) 4825–4835.
[13] M. Kaviany, M. Mittal, Int. J. Heat Mass Transfer 30 (1987) 1407–1418.
[14] J.A. Rogers, M. Kaviany, Int. J. Heat Mass Transfer 35 (1992) 469–480.
[15] G. Guillot, A. Trokiner, L. Darrasse, H. Saint-Jalmes, J. Phys. D: Appl. Phys. 22 (1989) 1646–1649.
[16] T.M. Shaw, Phys. Rev. Lett. 59 (1987) 1671.
[17] N. Shokri, P. Lehmann, P. Vontobel, D. Or, Water Resour. Res. 44 (2008) W06418.
[18] Y. Le Bray, M. Prat, Int. J. Heat Mass Transfer 42 (1999) 4207–4224.
[19] M. Prat, Chem. Eng. J. 86 (2002) 153–164.
[20] A.G. Yiotis, A.K. Stubos, A.G. Boudouvis, I.N. Tsimpanogiannis, Y.C. Yortsos, Transp. Porous Media 58 (2005) 63–86.
[21] A.G. Yiotis, I.N. Tsimpanogiannis, A.K. Stubos, Y.C. Yortsos, J. Colloid Interface Sci. 297 (2006) 738–748.
[22] N. Shahidzadeh-Bonn, A. Azouni, P. Coussot, J. Phys.: Condens. Matter 19 (2007) 112101.
[23] C. Quick, D. Ritzinger, W. Lehnert, C. Hartnig, J. Power Sources 190 (2009) 110–120.
[24] M. Kaviany, Principles of Heat Transfer in Porous Media, 2nd ed., Springer, 1995.
[25] F.P. Incropera, D.P. DeWitt, Fundamentals of Heat and Mass Transfer, 4th ed., John Wiley & Sons, New York, 1996.
[26] M.M. Mench, Fuel Cell Engines, John Wiley & Sons, Inc., Hoboken, 2008.
[27] S. Litster, N. Djilali, in: B. Sunden, M. Faghri (Eds.), Transport Phenomena in Fuel Cells, WIT Press, UK, 2005, pp. 175–213 (Chapter 5).
[28] K.T. Cho, Ph.D. Thesis, the Penn State University 2010.
[29] P. Coussot, Eur. Phys. J. B 15 (2000) 557–566.
[30] F. Barbir, PEM Fuel Cells: Theory and Practice, Elsevier Academic Press, San Diego, 2005.
[31] Y.A. Cengel, J.M. Cimbala, Fluid Mechanics: Fundamentals and Applications, McGraw Hill, New York, 2006.
[32] E.L. Cussler, Diffusion: Mass Transfer in Fluid Systems, Cambridge University Press, New York, 1984.
[33] M. Khandelwal, M.M. Mench, J. Power Sources 161 (2006) 1106–1115.
[34] Y.A. Cengel, M.A. Boles, Thermodynamics: An Engineering Approach, 4th ed., McGraw Hill, New York, 2001.